Growth and spectral properties of Nd^{3+}:$Li_3Ba_2La_3(WO_4)_8$ crystal

BIN XIAO[a,b], LIZHEN ZHANG[a], ZHOUBIN LIN[a],YISHENG HUANG[a], GUOFU WANG[a,*]
[a]*Key Laboratory of Optoelectronics Material Chemistry and Physics, Fujian Institute of Research on the Structure of Matter, Chinese Academy of Sciences, Fuzhou, Fujian 350003, China*
[b]*Graduate School of Chinese Academy of Sciences, Beijing 100037, China*

Nd^{3+}-doped $Li_3Ba_2La_3(WO_4)_8$ crystal with dimensions up to 21×56×6 mm^3 has been grown by the top seeded solution growth method (TSSG) from a flux of Li_2WO_4. The spectroscopic analysis of the Nd:LBLW crystal reveals that Nd: LBLW crystal has broad FWHM of absorption band and large absorption cross-section at 803 nm. The emission cross-sections of Nd: LBLW crystal are comparable to those for other Nd^{3+} crystals (see Table 3). The fluorescence quantum efficiency η is up to 95.7%. The analysis of spectral properties suggests the Nd:LBLW crystal as a potential candidate for solid-state laser materials for diode laser pumping.

(Received January 30, 2012; accepted April 11, 2012)

Keywords: Laser crystal, Crystal growth, Spectral properties, Nd^{3+}:$Li_3Ba_2La_3(WO_4)_8$ crystal

1. Introduction

With the development of high power laser diodes, the exploration new laser crystal has always received a great deal of attention. Nd^{3+}:YAG crystal is commercially available, but limited to low Nd^{3+}-doping concentration and narrow absorption band which has only absorption line width of 1 nm at 808 nm [1]. Therefore, the temperature stability of the output wavelength of diode laser needs to be seriously controlled by reason that the emission wavelength of the diode laser shifts with the temperature [2]. Some efforts have been made to find crystals with wide absorption line width such as Nd^{3+}:$CaWO_4$ [3], Nd^{3+}:$KY(WO_4)_2$ [4], and Nd^{3+}:$LiLa(WO_4)_2$ [5]. These crystals have broad absorption and emission bands, large absorption and emission cross sections, as well as high quantum efficiency, which make them promising solid-state laser materials [6].

The triple tungstate crystals with the general formula $Li_3Ba_2Ln_3(WO_4)_8$ (Ln=La-Lu,Y), which were discovered in our laboratory, also exhibit excellent spectroscopic and lasing characteristic for solid-state lasers [7]. They belong to the monoclinic system with space group *C*2/c with *a*=5.323(6) (Å), *b*=13.091(15) (Å), *c*=19.48(2) (Å), *β*=91.18(3)°, and *Z*=2 [8]. Previous study demonstrated existence of layered structure perpendicular to the *c* axis and two different and shared crystal sites for Ln^{3+} cations [9], which leads to locally disordered environments around Ln^{3+} ions. When Nd^{3+} ions, which are used as the active ions, are doped into the crystal and occupy the sites of Ln^{3+} ions, the different crystal fields around the Nd^{3+} ions induce the spectral broadening. Tunable and short pulse laser operations of these crystals can be expected since they have relatively broad absorption and emission bands [10-13]. Therefore, it is interesting to investigate the spectral properties of these Nd^{3+} doped disordered crystals.

In this work, the crystal growth, room-temperature polarized absorption and fluorescence spectra as well as fluorescence decay curve of the orientated Nd^{3+}:$Li_3Ba_2La_3(WO_4)_8$ (Nd^{3+}:LBLW) were investigated. The spectral parameters were investigated consistently with the anisotropic character of the crystal. The relation among the crystal structure, the crystal morphology, and the spectroscopic parameters was discussed.

2. Experiment

Nd:LBLW crystal was grown by the top seed solution growth (TSSG) method from a flux of Li_2WO_4. The Li_2WO_4 was chosen as a flux because it slows the viscosity of the solution and low melting point. To select the suitable composition of the solution, the solubility curve of LBLW in the $Li_3Ba_2La_3(WO_4)_8$-Li_2WO_4 solution was determined by means of trial seeding. The obtained result is shown in Fig. 1. The crystal growth was carried out a vertical tubular. Muffle finance with an AL-708 temperature controller and used a ϕ60×50 mm^2 platinum crucible. The starting materials with 25 mol% $Li_3Ba_2La_3(WO_4)$ doped Nd_2O_3 and 75 mol% Li_2WO_4 were weighed according to following the chemical reaction:

$$3Li_2CO_3+4BaCO_3+2.85La_2O_3+0.15Nd_2O_3+16WO_3=2Li_3Ba_2La_{2.85}Nd_{0.15}(WO_4)_8+7CO_2\uparrow \quad (1)$$

$$2LiCO_3+WO_4=Li_2WO_4+CO_2\uparrow \quad (2)$$

The chemicals used were Li_2CO_3, $BaCO_3$ and WO_3 with AR grade and La_2O_3 and Nd_2O_3 with 99.99% purity. The weighted raw materials were mixed and put into a ϕ60×50 mm^2 platinum crucible. Then the mixture was held at 1300K for 48 h to let the solution melt completely and homogeneously. Then, a Pt wire was used as a seed to contact the solution, and the solution temperature was slowly cooled down at a cooling rate of 30K/day. The small crystals grown on the Pt wire were obtained by spontaneous crystallization. The crystal cut as grown crystal with [001] orientation was used as seed to grow the larger crystal. The saturation temperature of the solution was determined exactly by repeated seeding. The crystal crystallization temperature was 1191 K. During the growth period, was slowly cooled at a rate of 1 K /day and rotated at a rate of 40 rpm. After two weeks, the grown crystal was pulled out from the solution and cooled down to room temperature at the rate of 15 ^{0}C/h.

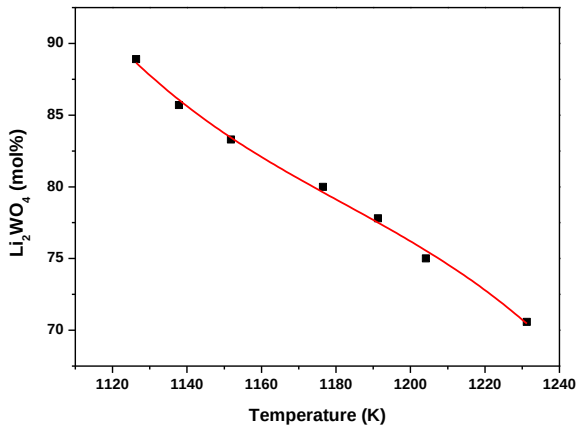

Fig. 1. Solubility curve of $Li_3Ba_2La_3(WO_4)_8$ in $Li_3Ba_2La_3(WO_4)_3$-Li_2WO_4 solution.

Using the crossed polarizing microscope and x-ray diffraction, the orientation of the crystal can be determined and the orientation procedure in similar to Ref. [14]. The optical indicatrix axes with regard to the crystallographic axes (a, b, c) is similar to that of Tm^{3+}:$Li_3Ba_2Lu_3(MoO_4)_8$ crystal [8]. A sample with dimensions of 5.8 mm × 4.5 mm × 3.7 mm was cut from the as-grown crystal for spectral experiments. Each face of sample was polished and perpendicular to one of the principal optical indicatrix axes (*X*, *Y*, *and Z*). The absorption spectra of Nd:LBLW were measured on a spectrophotometer (Lambda900, PerkinElmer UV/VIS/NIR) in the range of 300-950 nm with a step of 1.0 nm at room temperature. The polarized fluorescence spectra in the range of 850-1450 nm and the fluorescence decay curve at 1060 nm, corresponding to $^4F_{3/2}\rightarrow{}^4I_{11/2}$ transition were recorded using an Edinburgh Instruments FL920 spectrophotometer with xenon lamp as light source. In the experiment the incident light is parallel to the *X*-axis, *Y* -axis and *Z*-axis, respectively.

3. Results and discussion

3.1 Crystal growth

The Nd^{3+}LLBLW crystal with dimensions of 21×56×6 mm^3 was grown by the TSSG method, as shown in Fig. 2. The samples used to measure the Nd3+ ions concentration were cut from middle, bottom and edge of the as-grown crystal. The concentration of Nd^{3+} ions was determined to be 3.64 at% (1.68×10^{20} cm^{-3}) by the inductively coupled plasma atomic emission spectrometry (ICP-AES, Ultima2, Jobin-Yvon). The segregation coefficient K can be expressed as

$$K = C_{\mathrm{sol}}/C_{\mathrm{liq}} \quad (1)$$

where C_{sol} and C_{liq} are the concentrations of Nd^{3+} ions in the solid and liquid phases, respectively. Thus, the segregation coefficient of Nd^{3+} ions in the Nd^{3+}:LBLW crystal is 0.73. The X-ray power diffraction (XRD) pattern of the crystal was obtained from the diffractometer (DMAX2500, RIGAKU) equipped with a Cu K α radiation (λ=1.540 Å) in the range of 2θ=15-65°. The XRD pattern of Nd^{3+}:LBLW (see Fig. 3) is similar to those of Nd^{3+}:$Li_3Ba_2Gd_3(WO_4)_8$ [7].

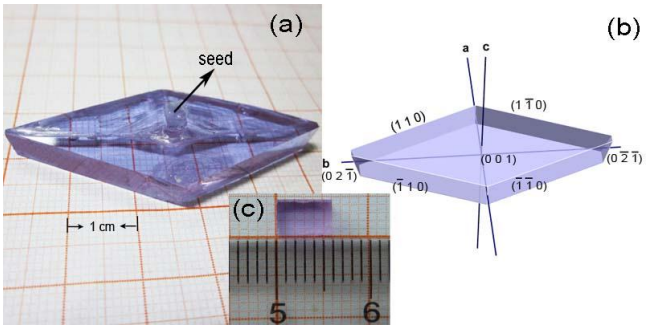

Fig. 2. Nd^{3+}:$Li_3Ba_2La_3(WO_4)_8$ crystal grown along [001] direction: (a) as-grown crystal with diamond-like shape; (b) facets marked by Miller indices (hkl); (c) a polished slice.

The grown transparency crystal with free inclusion exhibits good morphology. The morphology of the crystal is shown in Fig. 2 (b), which was simulated with Bravais-Friedel and Donnay-Harker based *WinXMorph* software. Nd^{3+}:LBLW crystal grown along *c*-oriented seed are surrounded by eight faces: (001), $(00\bar{1})$, (110), $(1\bar{1}0)$, $(\bar{1}10)$, $(\bar{1}\bar{1}0)$, $(02\bar{1})$, $(0\bar{2}\bar{1})$. The last two faces are less developed than others. This is probably due to the distinctive layered arrangement along *c* axis [9], which also makes Nd^{3+}:LBLW crystal have the diamond-like appearance.

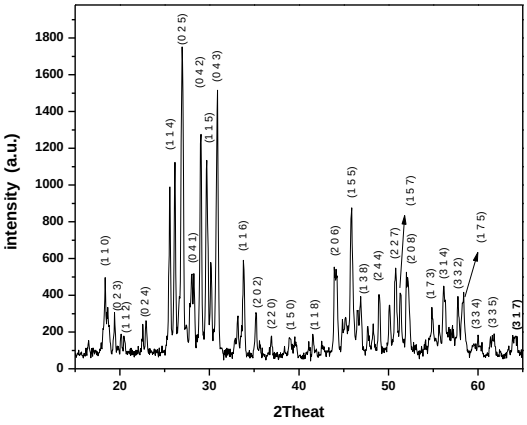

Fig. 3. X-ray power diffraction pattern of Nd^{3+}:LBLW crystal.

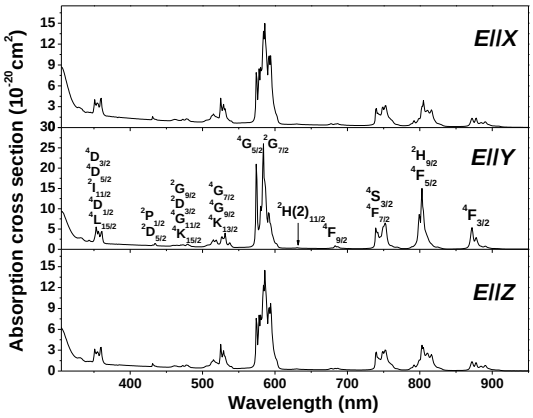

Fig. 4. Polarized absorption spectra of Nd^{3+}:LBLW crystal at room temperature.

3.1 Absorption spectra and Judd-Ofelt analysis

The polarized absorption spectra of Nd^{3+}:LBLW crystal is shown in Fig. 4. The absorption bands are attributed to transitions of Nd^{3+} from the ground state $^4I_{9/2}$ to the excited states. As can be seen, the absorption spectra are strongly polarization dependent due to the effect of anisotropy. In terms of the transition $^4I_{9/2} \rightarrow {}^4F_{5/2}+{}^2H_{9/2}$, the absorption band for *E*//*Y* has a markedly larger cross-section and a narrower bandwidth. The absorption cross-sections are 3.9×10^{-20} cm^2 at 805 nm for *E*//*X*, 15×10^{-20} cm^2 at 803 nm for *E*//*Y*, and 3.7×10^{-20} cm^2 at 803 nm for *E*//*Z*. The value of absorption cross-section for *E*//*Y* is also much larger than those of Nd^{3+}:YAG (7.3×10^{-20} cm^2) [1] and Nd^{3+}:$SrGdGa_3O_7$ (3.5×10^{-20} cm^2) [15]. It means that the plane coaxial with the *Y*-axis can be pumped more effectively. The absorption band at 803 nm has a broad full-width at half-maximum (FWHM) of 16 nm for *E*//*X*, 7 nm for *E*//*Y*, and 16 nm for *E*//*Z*., which are much broader than those of Nd^{3+}:YAG (1nm) [1] and Nd^{3+}:YVO_4 (2 nm) [16]. Such broad FWHM is caused by the statistical distribution of La^{3+} and Li^{3+} ions [9], which is suitable for the diode laser pumping because it is not crucial to temperature stability of the output wavelength of diode laser. Therefore, the large absorption cross-section and the broad FWHM at the pumping wavelength around 803 nm demonstrate that the Nd^{3+}:LBLW crystal can be pumped efficiently by the diode lasers.

The Judd-Ofelt (J-O) analysis model has become a standard method for analyzing the room-temperature absorption spectra of rare-earth ion-doped glasses and crystals. Ten absorption bands, corresponding to the transitions from the ground state $^4I_{9/2}$, were used to calculate the J-O parameters (see Table 1). For the Nd^{3+} ions, the absorptions caused by magnetic-dipole transitions have much weaker line strength than those caused by electric-dipole transitions and can be neglected in the J-O calculation [17]. The detailed calculation procedure is similar to that reported in [18]. The reduced matrix elements of unit tensor operator used in the calculation were taken from the existing literature [19]. The values of the measured and calculated line strength, denoted as S_{mca} and S_{cal} respectively, and the oscillator strength parameters $\Omega^{X,Y,Z}$ for each polarization are listed in Table 1. In table 1, Ω^{eff} is the effective oscillator strength parameter which is defined as $\Omega^{eff} = (\Omega^X + \Omega^Y + \Omega^Z)/3$. The root mean square deviations (RMS ΔS) from 1.6×10^{-21} cm^2 to 3.7×10^{-21} cm^2 are in the typical error range of J-O theory [20], which suggests that the calculated results are in consistent with the experimental data. It can be found that Nd^{3+}:LBLW has a high Ω_2 value because of the distorted environment [21] and the intensive absorption of the hypersensitive $^4I_{9/2} \rightarrow {}^4G_{5/2} + {}^2G_{7/2}$ transition around 587 nm [22]. This phenomenon has also been observed in some other tungstate crystals such as Nd^{3+}:$LiLa(WO_4)_2$ [5], $Nd^{3+}KY(WO_4)_2$ [4], and Nd^{3+}:$La_2(WO_4)_2$ [23].

Table 1. J-O Intensity parameters, measured and calculated line strengths for polarized spectra of Nd^{3+}:LBLW crystal at room temperature.

J'-Manifold	*E//X*			*E//Y*			*E//Z*		
	$\bar{\lambda}$ (nm)	$S(J\to J')(10^{-20}\mathrm{cm}^2)$		$\bar{\lambda}$ (nm)	$S(J\to J')(10^{-20}\mathrm{cm}^2)$		$\bar{\lambda}$ (nm)	$S(J\to J')(10^{-20}\mathrm{cm}^2)$	
		S_{mea}	S_{cal}		S_{mea}	S_{cal}		S_{mea}	S_{cal}
$^4F_{3/2}$	883	0.73	0.80	877	1.74	1.35	882	0.75	0.79
$^4F_{5/2}+^2H_{9/2}$	809	2.06	2.17	804	4.69	4.10	808	2.12	2.16
$^4F_{7/2}+^4S_{3/2}$	750	1.90	1.90	749	3.42	3.90	749	1.88	1.92
$^4F_{9/2}$	684	0.14	0.15	685	0.24	0.28	684	0.16	0.15
$^2H(2)_{11/2}$	630	0.03	0.03	629	0.04	0.07	630	0.03	0.03
$^4G_{5/2}+^2G_{7/2}$	586	11.28	11.31	584	13.66	13.67	586	10.67	10.70
$^2K_{13/2}+^4G_{7/2}+^4G_{9/2}$	524	2.09	1.61	524	2.57	2.43	524	1.95	1.56
$^2K_{15/2}+^2G_{9/2}+^2D_{3/2}+^4G_{11/2}$	471	0.34	0.23	473	0.48	0.41	472	0.33	0.23
$^2P_{1/2}+^2D_{5/2}$	433	0.09	0.11	433	0.17	0.18	433	0.08	0.10
$^4D_{3/2}+^4D_{5/2}+^2I_{11/2}+^4D_{1/2}+^2L_{15/2}$	356	1.69	1.78	356	2.46	2.89	356	1.64	1.74
RMS ΔS $(10^{-21}\,\mathrm{cm}^2)$		1.9			3.7			1.6	
$\Omega^{X,Y,Z}(10^{-20}\,\mathrm{cm}^2)$		9.6, 2.9, 2.7			10.9, 4.6, 5.6			9.0, 2.8, 2.7	
$\Omega^{eff}(10^{-20}\,\mathrm{cm}^2)$		9.8,			3.4			3.7	

Once the oscillator strength parameters have been obtained, the spontaneous emission probability A, the fluorescence branching ratio β of the fluorescence transitions to the lower-lying ^4I_J (J=15/2, 13/2, 11/2, 9/2) multiplets and the radiative lifetime τ_{rad} of the $^4F_{3/2}$ multiplet can be calculated. All these results for the main transitions of the Nd^{3+} ions in the LBLW crystal with different polarizations are listed in Table 2.

Table 2. Polarized spontaneous emission probabilities and fluorescence branching ratios for the $^4F_{3/2}\to{}^4I_J$ transitions of the Nd3+:LBLW crystal.

Transitions	E//X		E//Y		E//Z	
	A (S^{-1})	β (%)	A (S^{-1})	β (%)	A (S^{-1})	β (%)
$^4F_{3/2}\to{}^4I_{15/2}$	17.5	0.5	36.8	0.5	17.7	0.5
$^4F_{3/2}\to{}^4I_{13/2}$	341.5	9.1	707.0	1.2	342.8	9.3
$^4F_{3/2}\to{}^4I_{11/2}$	1728.2	46.3	3426.2	49.3	1716.2	46.4
$^4F_{3/2}\to{}^4I_{9/2}$	1648.6	44.1	2777.2	40.0	1624.7	43.9
$\tau_{\mathrm{rad}}\,(\mu\mathrm{s})$			209			

3. 3 Fluorescence spectra and lifetime

Fig. 5 illustrates the emission cross-sections at various wavelengths λ with different polarizations, which was calculated from the room-temperature polarized fluorescence spectra by the Füchtbauer-Ladenburg (F-L) formula [24],

$$\sigma_{F\text{-}L}^{q} = \frac{\lambda^5 A_q(J \to J') I_q(\lambda)}{8\pi c n^2 \int \lambda I_q(\lambda) \mathrm{d}\lambda} \qquad (2)$$

where $I_q(\lambda)$ is the fluorescence intensity at wavelength λ, q indicates the polarization of spectra, c is the speed of light in the vacuum and n is the refractive index of the crystal. Three emission bands corresponding to the $^4F_{3/2} \rightarrow {}^4I_{9/2}$, $^4F_{3/2} \rightarrow {}^4I_{11/2}$ and $^4F_{3/2} \rightarrow {}^4I_{13/2}$ transitions are observed at 855~922, 1030~1100 and 1300~1400 nm. In terms of the $^4F_{3/2} \rightarrow {}^4I_{11/2}$ laser channel, the emission bands are also strongly polarization dependent. The emission band for *E//Y* has a significantly larger stimulated cross-section. The stimulated emission cross-sections are 5.5×10^{-20} cm^2 at 1064 nm for *E//X*, 11×10^{-20} cm^2 at 1059 nm for *E//Y* and 5.7×10^{-20} cm^2 at 1064 nm for *E//Z*, which are comparable to other disordered crystals, such as Nd^{3+}:$KY(WO_4)_2$ (5.4×10^{-20} cm^2) [5], Nd^{3+}:$LiLa(WO_4)_2$ (6.9×10^{-20} cm^2) [4] and Nd^{3+}:$KY(MoO_4)_2$ (15.4×10^{-20} cm^2) [25]. The FWHM of the emission band is 19 nm at 1064 nm, 16 nm at 1059 nm and 15 nm at 1063 nm for E//X, E//Y, E//Z, respectively, which are much larger than those of Nd^{3+}:YAG (0.8 nm) [1] and Nd^{3+}:$Ca_9Gd(VO_4)_7$ (10 nm, for π polarization) [26]. The broad FWHM is favorable for the generation of self-stimulated Raman laser because it benefits the generation of tunable and ultrashort pulse lasers with high peak power [27].

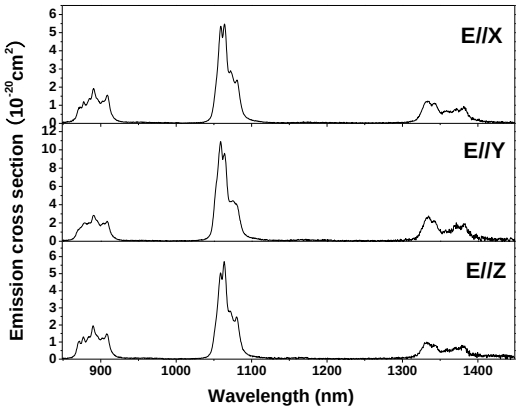

Fig. 5. Polarized emission spectra of Nd^{3+}:LBLW crystal excited 805 nm radiation at room temperature.

The fluorescence decay curve of the $^4F_{3/2}$ multiplet of the Nd^{3+}:LBLW crystal is shown in Fig. 6. The linear relationship in the figure displays single exponential behavior of the fluorescence decay. The fluorescence lifetime of the $^4F_{3/2}$ multiplet could be obtained from the slope of the fitting line k, i.e. τ_f=-1/(2.303k)=200 μs. Considering the inherent uncertainty of the J-O theory (approximately $+$20%) [20] and the different optical qualities and Nd^{3+} concentration of the grown crystals, it is reasonable that the fluorescence lifetime is a little higher than that of Nd^{3+}:$Li_3Ba2Gd_3(WO_4)_8$ (153 μ s) [7]. Combining the value of τ_r listed in Table 2, the fluorescence quantum efficiency, which is defined as $\eta = \tau_f/\tau_r$, is calculated to be 95.7%. The high quantum efficiency (close to unity) in Nd^{3+}:LBLW suggests that the non-radiative transition process from this multiplet can be nearly neglected. This is due to the relatively small phonon energy of the $(WO_4)^{2-}$ group ($\sim$900 cm^{-1}) [28] as well as the high optical quality of the crystal. Therefore, the laser performances of the Nd^{3+}:LBLW crystal can be improved because the thermal load triggered by the nonradiative transition from the $^4F_{3/2}$ of the crystal can be eliminated.

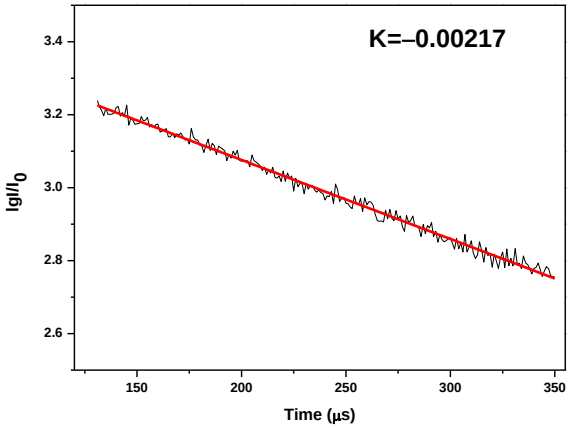

Fig. 6. Fluorescence decay curve at 1060 nm corresponding to $^4F_{3/2} \rightarrow {}^4I_{11/2}$ transition of Nd^{3+}:LBLW crystal excited 803 nm radiation.

Table 3 lists the main spectral parameters of the Nd^{3+}:LBLW crystal and some other Nd^{3+}-doped crystals. It can be seen that the most spectral parameters of the Nd^{3+}:LBLW crystal are similar to those of the isostructural Nd^{3+}:$Li_3Ba_2Y_3(WO_4)_8$, except that the measured fluorescence and radiative life time of the Nd^{3+}:LBLW crystal is 200 and 209 μs and longer than those of the Nd^{3+}:$Li_3Ba_2Y_3(WO_4)_8$ crystal (151 and 161 μ s, respectively), which may further due to the interactions between Nd^{3+} ions in the host, i.e., concentration quenching effect in addition to the above analysis. Moreover, the absorption and emission cross sections of both crystals are larger than those of the ordered crystals (YVO4,YAG and LaVO4, see Table 3 for details). Therefore, it can be predicted that the spectral properties of Nd^{3+}:LBLW crystal is comparable to those of the well known Nd^{3+}-doped crystals.

Table 3. Comparison of spectroscopy properties of the Nd^{3+}:LBLW crystal with other well-known crystals.

Crystal	Intensity parameters				Absorption ($^4I_{9/2}\rightarrow{}^4F_{5/2}+{}^2H_{9/2}$)		Emission ($^4F_{3/2}\rightarrow{}^4I_{11/2}$)					
	Ω_2	Ω_4	Ω_6	N_0	FWHM	Peak σ^{abs}	FWHM	Peak σ^{em}	τ_f	τ_r	η	Ref.
	(10^{-20} cm^2)			(10^{20}cm^{-3})	(nm)	(10^{-20}cm^2)	(nm)	(10^{-20}cm^2)	(μs)	(μs)	(%)	
LBLW	9.8	3.4	3.7	1.68	10 (*E*//*Y*)	15	16(*E*//*Y*)	11	200	209	95.7	This work
YVO_4	5.88	4.08	5.11	1.25	2 (π)	8	3.5	29.5	84	90	93.3	[16,29]
YAG	0.2	2.7	5.0	1.52	1	5.6	0.6	28	220	255	86.3	[30]
$KY(WO_4)_2$	8.8	3.11	3.16	2.90	4	5.8	15	5.39	154	196	78.6	[4, 31]
$LaVO_4$	2.1	3.9	3.2	4.15	20	3	13.3	6.1	137	209	65.6	[32,33]
$Li_3Ba_2Y_3(WO_4)_8$	11.7	4.8	4.3	2.22	17 (*E*//*Y*)	10	-	15.6	151	161	97.3	[9, 34]

4. Conclusion

Nd:LBLW crystal with dimensions up to 21×56×6 mm^3 was successfully grown from the flux of Li_2WO_4. The spectroscopic analysis of the Nd:LBLW crystal reveals that Nd:LBLW crystal has broad FWHM of absorption band and large absorption cross-section at 803 nm, which is suitable for diode laser pumping. The emission cross-sections of Nd:LBLW crystals are comparable to those for other Nd^{3+} crystals (see Table 3). The fluorescence quantum efficiency η is up to 95.7%, which can decrease crystal thermal load. Therefore, the investigated results suggest the Nd:LBLW crystal as a potential candidate for solid-state laser materials.

Acknowledgements

This work is supported by the National Natural Science Foundation of China (No. 61108054) and the National Natural Science Foundation of Fujian Province (No. 2011J01376), respectively.

Reference

[1] J. Lu, M. Prabhu, J. Song, C. Li, J. Xu, K. Ueda, A. A. Kaminskii, H. Yagi, T. Yanagitani, Appl. Phys. B: Lasers Opt. **71**, 469 (2000).
[2] W. Zhao, Z. B. Lin, L. Z. Zhang, G. F. Wang, J. Alloys Compd. **509**, 2815 (2011).
[3] A. A. Kaminskii, H. J. Eichler, K. Ueda, N. V. Klassen, B. S. Redkin, L. E. Li, J. Findeisen, D. Jaque, J. García-Sole, J. Fernández, R. Balda, Appl. Opt. **38**, 4533 (1999).
[4] X. Han, G. Wang, J. Crystal Growth **247,** 551 (2003).
[5] X.Y. Huang, Q. Fang, Q. M. Yu, X. D. Lue, L. Z. Zhang, Z. B. Lin, G. F. Wang, J. Alloys Compd. **468,** 321 (2009).
[6] V. Volkov, C. Cascales, A. Kling, C. Zaldo, Chem. Mater. **17,** 291 (2005).
[7] H. Li, L. Z. Zhang, G. F. Wang, J. Alloys Compd. **478,** 484 (2009).
[8] Y. Pan, Y. J. Chen, Y. F. Lin, X. H. Gong, J. H. Huang, Z. D. Luo, Y. D. Huang. CrystEngComm, **DOI:** 10.1039/C2CE25190F.
[9] H. Li, G. J. Wang, L. Z. Zhang, Y. S. Huang, G. F. Wang, CrystEngComm **12,** 1307 (2010).
[10] M. H. Ober, E. Sorokin, I. Sorokina, F. Krausz, E. Wintner, I. A. Shcherbakov, Opt. Lett. **17,** 1364 (1992).
[11] E. Sorokin, M. H. Ober, I. Sorokina, E. Wintner, A. J. Schmidt, A. I. Zagumennyi, G. B. Loutts, E. W. Zharikov, I. A. Shcherbakov, J. Opt. Soc. Am. B **10,** 1436 (1993).
[12] M. O. Ramírez, J. J. Romero, P. Molina, L. E. Bausá, Appl. Phys. B: Lasers Opt. **81,** 827 (2005).
[13] T. T. Basiev, N. A. Es'kov, A.Y. Karasik, V. V. Osiko, A. A. Sobol, S. N. Ushakov, M. Helbig, Opt. Lett. **17,** 201 (1992).
[14] M. Rico, X. Han, C. Cascales, F. Esteban-Betegón, C. Zaldo, Opt. Express, **19**, 7640 (2011).
[15] G. J. Quarles, L. Esterowitz, G. H. Rosenblatt, M. H. Randles, J. E. Creamer, R. F. Belt, Proc. SPIE **1863,** 74 (1993).
[16] Y. Sato, T. Taira, IEEE J. Sel. Top. Quantum Electron. **11,** 613 (2005).
[17] Y. J. Chen, X. Q. Lin, Z. D. Luo, Y. D. Huang, Chem. Phys. Lett. **397,** 282 (2004).
[18] M. J. Song, G. J. Wang, Z. B. Lin, L. Z. Zhang, G. F. Wang, J. Crystal Growth **308,** 208 (2007).
[19] W. T. Carnall, P. R. Fields, K. Rajnak, J. Chem. Phys. **49,** 4424 (1968).

[20] F. Cornacchia, A. Toncelli, M. Tonelli, E. Cavalli, E. Bovero, N. Magnani, J. Phys.: Condens. Matter. **16,** 6867 (2004).
[21] L. H. C. Andrade, D. Reyes Ardila, J. P. Andreeta, M. Siu Li, Opt. Mater. **22,** 369 (2003).
[22] X. Gong, Y. Chen, Y. Lin, Z. Luo, Y. Huang, J. Opt. Soc. Am. B **26,** 259 (2009).
[23] Y. J. Chen, X .Q. Lin, Z. D. Luo, Y. D. Huang, Chem. Phys. Lett. **381,** 598 (2003).
[24] B. Aull, H. Jenssen, IEEE J. Quantum Electron. **18,** 925 (1982).
[25] Y. Chen, Y. Lin, X. Gong, Q. Tan, Z. Luo, Y. Huang, J. Opt. Soc. Am. B **24,** 496 (2007).
[26] L.Y. Li, G. J. Wang, Y. S. Huang, L. Z. Zhang, Z. B. Lin, G. F. Wang, J. Crystal Growth **314**, 331 (2011).
[27] W. Koechner, Solid-State Laser Engineering, Springer-Verlag (1992).
[28] L. Macalik, J. Hanuza, A.A. Kaminskii, J. Mol. Struct. **555**, 289 (2000).
[29] T. S. Lomheim, L. G. De Shazer, Phys. Rev. B **20**, 4343 (1979).
[30] W. Krupke, IEEE J. Quantum Electron. **7,** 153 (1971).
[31] X. M. Han, L. Z. Zhang, M. W. Qiu, G. F. Wang, Mater. Res. Innovat. **7,** 355 (2003).
[32] L. Z. Zhang, Z. S. Hi, Z. B. Lin, G. F. Wang, J. Crystal Growth **260,** 460 (2004).
[33] L. Z. Zhang, M. W. Qiu, M. J. Song, G. F. Wang, Mater. Res. Innovat. **14**, 119 (2010).
[34] H. Li, G. Wang, L. Zhang, Y. Huang, G. Wang, Mater. Res. Innovat., **14**, 419 (2010).

*Corresponding author: wgf@ms.fjirsm.ac.cn